Low Temperature Physics/Fizika Nizkikh Temperatur, 2019, v. 45, No. 3, pp. 363–370

Theoretical study of “trapping sites” in cryogenic rare gas solids doped with β-dicarbonyl molecules

G. Rojas-Lorenzo[1], M. Lara-Moreno[2], A. Gutiérrez-Quintanilla[1,3], M. Chevalier[3], and C. Crépin[3]

[1]*Instituto Superior de Tecnologías y Ciencias Aplicadas (InSTEC), Universidad de La Habana, Ave. Salvador Allende No. 1110, Quinta de los Molinos, La Habana 10400, Cuba*

[2]*Université de Bordeaux and CNRS, ISM, UMR 5255, F-33400 Talence, France*

[3]*Institut des Sciences Moléculaires d'Orsay (ISMO), UMR 8214, CNRS, Univ. Paris-Sud, Université Paris Saclay, F-91405 Orsay, France*

E-mail: german@instec.cu;
claudine.crepin-gilbert@u-psud.fr

Received October 24, 2018

A deposition model to simulate the growth of doped rare gas crystals is used. The study involves organic molecules with a single intramolecular hydrogen bond such as malonaldehyde, 2chloromalonaldehyde and acetylacetone as impurities. Different trapping sites were obtained depending on the rare gas properties for a given impurity, and depending on the molecular size and shape for a given crystal. Simulations were carried out by using classical molecular dynamics methods including an anharmonic thermal correction, to take into account the zero point movement of the crystal. The results are correlated to spectroscopic data previously achieved for these systems by steady state IR spectroscopy.

Keywords: rare gas crystal, atomic and molecular impurities, interatomic pair potential, spectroscopy.

1. Introduction

Site effects play an important role in the spectroscopy of atomic and molecular impurities trapped in cryogenic solids [1–9]. Their influence is connected with the observation for a single vibrational mode or a single vibronic transition, of several bands in absorption and emission and with the shapes of the bands [1–3,10]. In presence of different trapping sites it is a difficult task to separate the individual spectroscopic contribution of each site. Several experimental and theoretical methods have been developed and used for this purpose [1–10]. Among them, molecular dynamics (MD) represents an useful tool to describe cryogenic crystals. The development of different theoretical models to reproduce the growth process of rare gas (RG) matrices with atomic or molecular impurities brings more insight into the study of trapping sites and their effects on the spectroscopy of these systems [4–9].

The alignment of a planar molecular impurity along a specific crystallographic plane was described for naphthalene, anthracene and porphyrin by applying a deposition model [6,7,9]. The site effects of the trapped atomic sodium in RG matrices have also been studied by similar methods [8]. In these four systems, the comparison with spectroscopic experimental data has confirmed the helpfulness of this simulation method. A brief discussion on the effect of trapping sites in the spectroscopy of malonaldehyde (MA) in comparison with 2chloromalonaldehyde (2ClMA) when they are embedded in Ar matrices has been previously presented [10]. A similar deposition model was used in that recent study.

The motivation for the present theoretical work on MA/RG, 2ClMA/RG and acetylacetone (AcAc)/RG matrices stems from the fact that these systems offer an opportunity to analyze site effects in two directions: (1) for a given organic molecule (OM) this study should address the influence of the rare-gas properties, such as the nearest neighbor distance and the range of the OM-RG interactions; (2) for a given rare gas matrix it should offer the possibility to evaluate the influence of the size and shape of the OM in OM/RG cryogenic crystals.

2. Methodology

2.1. Deposition model

The growth of the rare gas crystals was described by classical molecular dynamic simulations. A deposition model successfully applied in previous works was chosen [4–9].

Simulations of the experimental growing process by modeling assist our understanding of how the environment surrounds the accommodated impurity in the solid state and allow identifying the trapping sites.

The use of pair potentials in the description of the system does not allow the formation of a fcc structure of a pure RG matrix from the gas phase [11–13]. For that reason, a specific layer template is considered in the model in order to build a crystal with a specific structure. In our case a template of rare gas atoms ordered in a fcc structure was used as an initial target. The template is formed by 4 atomic layers. The atoms forming the first layer are fixed in their coordinates during the simulation in order to avoid rotational and translational motion of the lattice during the deposition process. The second atomic layer is thermalized by rescaling the velocities, acting then as a thermal bath. The atoms of the third and fourth layers are free to move within the constraints of the applied force field.

Templates reproducing (001) and (111) crystallographic planes with 72 (001) and 64 (111) RG atoms per layer were used. The layers were ordered along z axis, parallel to xy plane. Periodic boundary conditions in x and y directions were applied to simulate an infinite surface. The (001) fcc template corresponds to $5\times5\times2$ cell units, while (111) fcc template to $8\times4\times2$ cell units, summing, respectively, 288 and 384 atoms.

Projectiles (586 rare gas atoms and the molecular impurity) were shot at the target (the template) at constant velocity along the z direction. Their x, y initial positions were randomly generated covering uniformly all (x, y) surface of the target. Initial z values were the same for all projectiles and far enough from the target to guarantee that the projectile — target interactions can be considered as negligible at the beginning of the motion. The initial velocities of projectiles were based on the average velocity of each rare gas at 300 K. In all cases the projectiles started to move in a sequential way with a time delay of 5 ps between two consecutive shots. This parameter was set by varying its value between 1 and 20 ps, and observing convergence after 5 ps. Other works report different values between 1 and 200 ps [4–9]. The molecule was randomly projected onto the target among the first 72 projectiles with also a random spatial orientation.

2.2. Molecular dynamics

The interatomic interactions RG–RG were described by Lennard-Jones (LJ) pair potentials [14]. These RG–RG potentials have been successfully used in the description of periodic RG matrices [15,16]. Intramolecular interactions taking place inside the molecular impurities were described by CFF force field for bonding, planar angle and dihedral angle potentials [17,18]. The CFF has the parameters needed to describe the employed molecules. The RG–RG LJ potentials were fitted to the analytical nonbonded van der Waals potentials 9–6 included in the CFF force field, in order to obtain the parameters that describe the interactions of RG atoms with the atoms of the trapped molecules, using the CFF combining rules [17,18].

Thermal anharmonic (Ne) and harmonic (Ar, Kr and Xe) quantum corrections were applied in order to take into account the zero point energy (ZPE) in the classical approach used for describing the real process at 7 K. Effective temperatures of 17, 46, 36 and 31 K were used in Ne, Ar, Kr and Xe, respectively [19,20]. As far as the authors know, this kind of corrections has not been considered in other reports on deposition models. The thermal anharmonic quantum correction was developed for RG–RG LJ pair potentials. For that reason LJ potentials were used to describe RG–RG interactions.

The equation of motion was integrated using the Verlet algorithm within a time step of 1 fs.

2.3. Molecular impurities

The three impurities studied in this work were molecules belonging to the β-dicarbonyl family in their chelated enol form. The simplest molecule was malonaldehyde (MA, $C_3O_2H_4$). The second molecule was 2chloromalonaldehyde (2ClMA, $C_3O_2H_3Cl$), which is obtained from MA by substituting the olefinic hydrogen by a chlorine. The most challenging impurity was acetylacetone (AcAc, $C_5O_2H_8$). These three molecules have a high degree of double bond resonance, which enhances the strength of the intramolecular hydrogen bond involving the two oxygens. Due to this effect, their backbones have a planar configuration. In the case of AcAc, two of the hydrogen atoms in each methyl groups are out of the backbone plane. The main structural details of these impurities are presented in Fig. 1.

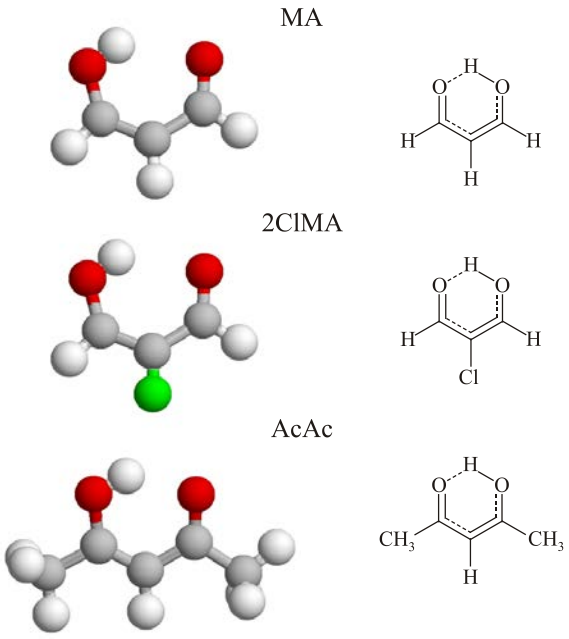

Fig. 1. (Color online) Structure of malonaldehyde (MA), 2chloromalonaldehyde (2ClMA) and acetylacetone (AcAc) molecules. Carbons are presented in grey, oxygen atoms in red, chlorine in green and hydrogen atoms are white.

The molecular masses vary in the following order MA (72 uma), AcAc (100 uma) and 2ClMA (106 uma). From a geometrical point of view, MA and 2ClMA are similar, while AcAc has the largest volume.

3. Results

The simulations were carried out by generating 100 samples for each impurity in Ne, Ar, Kr and Xe matrices, for both used templates. No dependence on the template used was observed in obtaining the trapping sites, *i.e.*, the results were similar with the two templates. A bigger number of samples (1000) was applied in the case of AcAc to check the statistics. No improvement was observed under such conditions. The structural properties of the samples were analyzed by means of the alignment of the molecular impurity along some preferred crystallographic planes. Figure 2 shows the relative population in preferred crystallographic planes for each molecule in the different rare gas matrices. The population distribution clearly shows that the three molecules under study are mainly trapped in two crystallographic planes: (001) and (111). This behavior is not surprising if we take into account the structural similarities of the three molecular guests. The population of other crystallographic planes is almost negligible, except for AcAc which presents two bulky methyl groups.

The vacancies are labeled as *n*v, where *n* is the number of rare gas atoms that is necessary to remove from a perfect crystal in order to trap the impurity: 1v for a single vacancy, 2v for two removed rare gas atoms, 3v for three removed rare gas atoms, and so on. Different examples of vacancy sites obtained in the simulations are shown in Fig. 3. The geometrical characteristics of typical vacancy sites formed in (001), (111) and (110) main planes are presented in this figure.

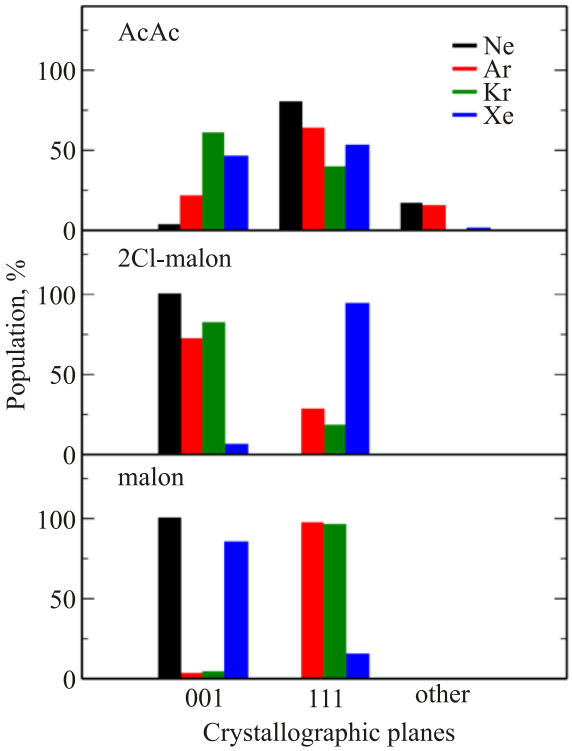

Fig. 2. (Color online) Relative population of preferred crystallographic planes for malonaldehyde (malon), 2chloromalonaldehyde (2Cl-malon) and acetylacetone (AcAc) molecules in Ne, Ar, Kr and Xe solid matrices.

3.1. Ne *matrices*

100% of MA and 2ClMA molecules are located along (001) planes, while only 3% of AcAc molecules prefer to be aligned along this plane. MA is trapped in 4v sites, 2ClMA in 5v sites and AcAc in 6v sites of (001) planes. The molecules are flexible in our MD simulations, and in

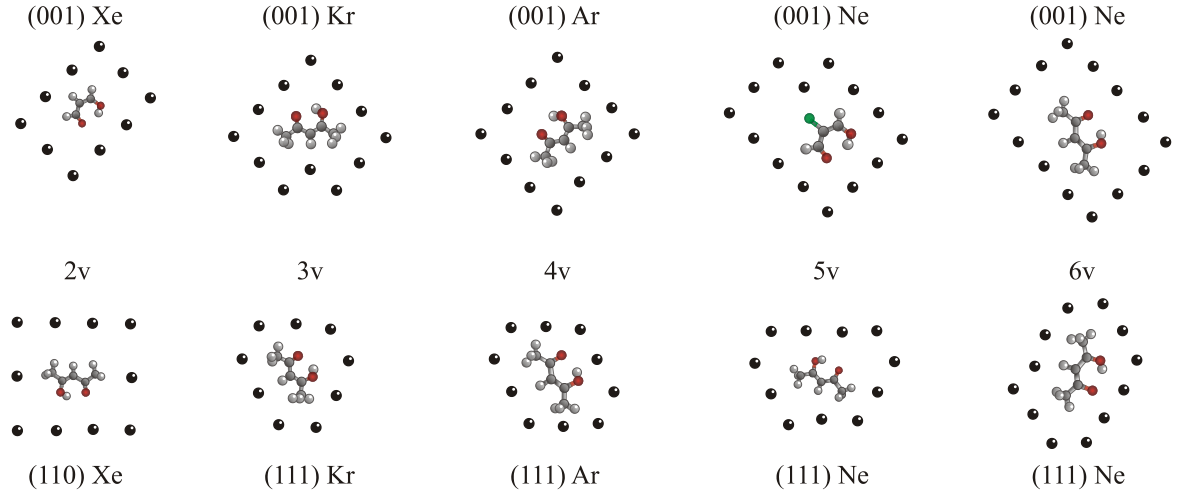

Fig. 3. Representation of different vacancy sites observed in (001), (111) and (110) crystallographic planes of the rare gas crystals. The nearest RG neighbors of the impurity are shown with black solid circles. In all cases AcAc is shown as the impurity except in cases 2v (001) Xe, and 5v (001) Ne, where the impurities are MA and 2ClMA, respectively.

Table 1. Relative population of preferred crystallographic planes for each impurity in the rare gas solids under study. The most populated sites are presented in bold type for each molecule in each plane. The number of RG atoms removed from adjacent parallel crystallographic planes (up to +2 or +3) is reported in all the cases

	Ne			Ar			Kr			Xe		
	MA	2ClMA	AcAc	MA	2ClMA	AcAc	MA	2ClMA	AcAc	MA	2ClMA	AcAc
(001)	100	100	3	3	72	21	4	82	61	85	6	46
site	**4v+2**	**5v+2**	**6v+3**	**3v+1**	**4v+2**	**3v+2**	3v, **4v**	**4v**	**3v**, 4v+**1**	**2v**	**3v**	**3v**
(111)	0	0	80	97	28	64	96	18	39	15	94	53
site	–	–	**5v+2**	**3v+1**	**3v+1**	4v, **5v+1**	**3v**	3v+**1**	3v, **4v**, 5v	**3v**	**3v**	**3v**, 4v
other	–	–	17	–	–	15	–	–	–	–	–	1
site	–	–	–	–	–	–	–	–	–	–	–	**2v** (110)

few cases (10%) C atoms of MA molecule are out of (001) plane while in almost all cases (80%) Cl atom of 2ClMA molecule is out of the (001) plane. As the Ne crystal has the shortest lattice parameter, it is necessary to remove more rare gas atoms in Ne than in the other heavier rare gas matrices to accommodate the impurities. For all three molecules 1, 2 and even 3 vacancies are formed in the nearest (both sides) planes parallel to the main plane containing the impurity. This effect is pronounced for AcAc due the hydrogens of the methyl groups.

The picture is quite different in the (111) crystallographic plane. The AcAc molecules prefer trapping in (111) planes forming 5v sites in 80% of cases. The details are presented in Table 1, as well as in Fig. 2. In all cases the nearest surrounding Ne atoms are displaced 0.6–1.0 Å from their equilibrium positions in the pure Ne solid. This is a clear indication that the repulsive zone of the interatomic potential is reached.

3.2. Ar *matrices*

In 97% of the samples, the Ar solid growth up with MA aligned along (111) planes, and only 3% along (001) planes, forming in both cases 3v sites. 2ClMA prefers to be accommodated along (001) planes in 72% of samples, while in the other 28% it is located along (111) planes forming 4v and 3v sites, respectively. In the case of AcAc, the impurity is located along (001) planes forming 3v sites in 21% of the samples, along (111) planes forming 5v sites in 64% of the samples, and in 15% of cases it appears in a plane in between (001) and (111). Moreover, the formation of 1 vacancy in a nearest plane parallel to the plane containing the impurity is observed for each molecule. The details are presented in Table 1, as well as in Fig. 2.

3.3. Kr *matrices*

The MA molecule was found in 96% of the Kr crystals laying on (111) planes forming 3v sites, and 4% in (001) planes forming 3v and 4v sites. Crystals trapping 2ClMA show the impurity accommodated along (001) planes in 82% of the cases, forming only 4v sites, and along (111) planes in 18% of the samples forming 3v sites in the main plane and 1 vacancy in a parallel nearest crystallographic plane. AcAc prefers to be located along (001) plane in 61% of depositions forming 3v (64%) and 4v (36%) sites, and along (111) planes in 39% of the cases forming 3v (27%), 4v (45%) and 5v (28%) sites. Details are presented in Table 1, as well as in Fig. 2.

3.4. Xe *matrices*

The Xe solids show the largest nearest neighbor distance in the studied rare gas crystals. In this solid MA is trapped in (001) planes in 85% of the crystals forming 2v sites, and in (111) planes forming 3v sites in the other 15% of depositions. 2ClMA prefers to be located along (111) planes in 94% of the samples, and along (001) planes in the other 6% of the cases, forming only 3v sites in both planes. In the case of AcAc the trapped molecules is aligned along (111) planes in 53% of depositions and along (001) planes in 46% of the samples, forming 3v sites in both cases. 1% of the simulated crystals shows the molecule in (110) planes forming 2v sites. Details are presented in Table 1, as well as in Fig. 2.

4. Discussion

Important geometric parameters of fcc rare gas solids are reported in Table 2: the nearest neighbor distances, r_{nn}, as well as the $d_{(001)}$, $d_{(111)}$ and $d_{(110)}$ distances between the adjacent (001), (111) and (110) crystallographic planes, respectively.

Table 2. Geometrical parameters of equilibrated rare gas solids. Distances are reported in Å. r_{nn} is the nearest neighbor distance; $d_{(ijk)}$ is the distance between adjacent parallel crystallographic planes (*ijk*)

	r_{nn}	$d_{(001)}$	$d_{(111)}$	$d_{(110)}$
Ne	3.13	2.21	2.50	1.57
Ar	3.76	2.66	3.03	1.88
Kr	4.01	2.84	3.25	2.01
Xe	4.35	3.08	3.56	2.18

The biggest vacancy sites 4v, 5v and 6v are formed in the (001) planes for Ne matrices, where r_{nn} is the shortest distance in the studied rare gas series (see Table 1). In this matrix MA occupies a 4v site, while a massive 2ClMA needs a 5v site to be accommodated along (001) plane and the largest AcAc molecule forms a 6v site. In contrast to AcAc molecule that prefers to be located along (111) planes, MA and 2ClMA molecules are not found aligned along these planes. The methyl hydrogens of AcAc which are out of the backbone plane strongly interact with the Ne atoms of the nearest parallel planes. This kind of interaction explains the fact that AcAc prefers to be located in planes where the distance between them is bigger, *i.e.*, (111) planes. The increase of r_{nn} in heavier rare gas matrices, and the subsequent increment of distances between planes, show a competition between (001) and (111) planes as the preferred plane where the AcAc molecule is located. In all matrices AcAc prefers (111) planes, except in Kr matrices, but the population in these planes is still significant (39%).

As expected, the number of rare gas atoms removed in the vacancy sites decreases when r_{nn} increases. This is the case of MA trapped mainly in 4v (001), 3v (111), 3v (111) and 2v (001) sites in Ne, Ar, Kr and Xe matrices, respectively. With 2ClMA a repulsive interaction of Cl atom with Ne is observed: the equilibrium position of Cl–RG is at a much larger distance than r_{nn} in Ne (3.61 Å). It is only slightly larger than r_{nn} in Ar (3.89 Å) matrices (see Fig. 4). Conversely, the interaction of the Cl atom with Kr and Xe atoms is attractive. The dependence of this interaction on RG together with the increment of the RG–RG distance from Ne to Xe are key points in the resulting trapping sites of 2ClMA which are 5v (001), 4v (001), 4v (001) and 3v (111) in Ne, Ar, Kr and Xe matrices, respectively. In the case of AcAc, the most populated sites are 5v (111), 5v (111), 3v (001) and 3v (111) in Ne, Ar, Kr and Xe matrices, respectively. The formation of 1, 2, and 3 vacancies in nearest parallel planes is observed in Ne matrices due to the repulsion that exert the methyl hydrogens on Ne atoms, as mentioned above. Due to the largest $d_{(ijk)}$ distances in the case of Xe, all the three impurities are embedded in crystallographic planes without removing any other Xe atoms from nearest planes. It can be the case in Kr, but it depends on the impurity (easier for MA than for AcAc and 2ClMA) and the trapping plane (Table 1).

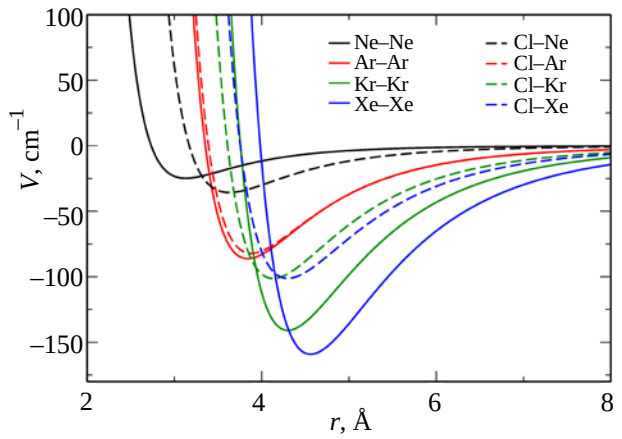

Fig. 4. (Color online) Interatomic pair potentials RG–RG and RG–Cl.

How much the impurity distorts its environment when it is trapped in cryogenic solids is a key question to be solved in order to understand the spectroscopic data. A comparison of the extent of the perturbation due to AcAc in the different rare gas matrices is shown in Fig. 5. The radial distribution function $g(r)$ describing the order of RG atoms inside the crystal is presented. It is important to note that the largest deviations occur in Ne matrices. This effect was also observed in rare gas crystals doped with MA and 2ClMA molecules, but less marked than in the case of AcAc. The delocalization and the extension of the perturbation decrease with the augmentation of the rare gas mass, *i.e.*, from Ne to Xe.

The $g(r)$ function presented in Fig. 5 for Ar and Kr crystals doped with AcAc shows a splitting of the second and fifth bands, as a consequence of the local deformation introduced by the impurity in the cryogenic solid. The deviation experienced by Ne atoms from their positions in the pure solid, laying at different distances from the impurity, are shown on the right panel by means of red asterisks. The rearrangement of Ne atoms in some crystallographic directions (pointed in Fig. 5 with arrows) could be responsible for that splitting, which is stronger in Ne and Ar and weaker, but very well defined, in Kr matrices.

An histogram of "solvation" energies inside a 6×6×4 matrix block (LJ interaction energy between the guest molecule and all RG atoms of the solid) [9] is presented in Fig. 6.

A single band is observed for MA in Ne corresponding to 4v+2 (001) sites. The MA–RG interactions are stronger in Ar than in Ne resulting in two bands at lower energies. The minor one is almost imperceptible and corresponds to 3v+1 (001) sites, while the major one is associated to 3v+1 (111) sites. The intensities of these bands are correlated to the data shown in Table 1. In the case of Kr matrices two bands at lower energies in comparison with Ar bands, are observed, as expected because of stronger MA–Kr interactions. The small band has a complex structure and is correlated to 3v and 4v (001) sites while the major one corresponds to 3v (111) sites.

The site contribution to solvation energies in Xe matrices shows an interesting behavior. The bands of MA in Xe (blue line in the bottom panel of Fig. 6) appear close to the contribution in Ar matrices (red line), with a minor band correlated to 3v (111) sites and a major band, at higher energy, correlated to 2v (001) sites. This fact could be explained by the values of the equilibrium position in the pair potentials and the Xe–Xe distance (see Fig. 7). The main contributions to MA–RG interactions (O–RG, C–RG and H–RG), and the RG–RG potential are presented in Fig. 7: RG = Ar in the left panel, RG = Kr in the middle panel and RG = Xe in the right panel. The Ar–Ar, O–Ar and C–Ar equilibrium positions in the interaction potentials are very close to each other.

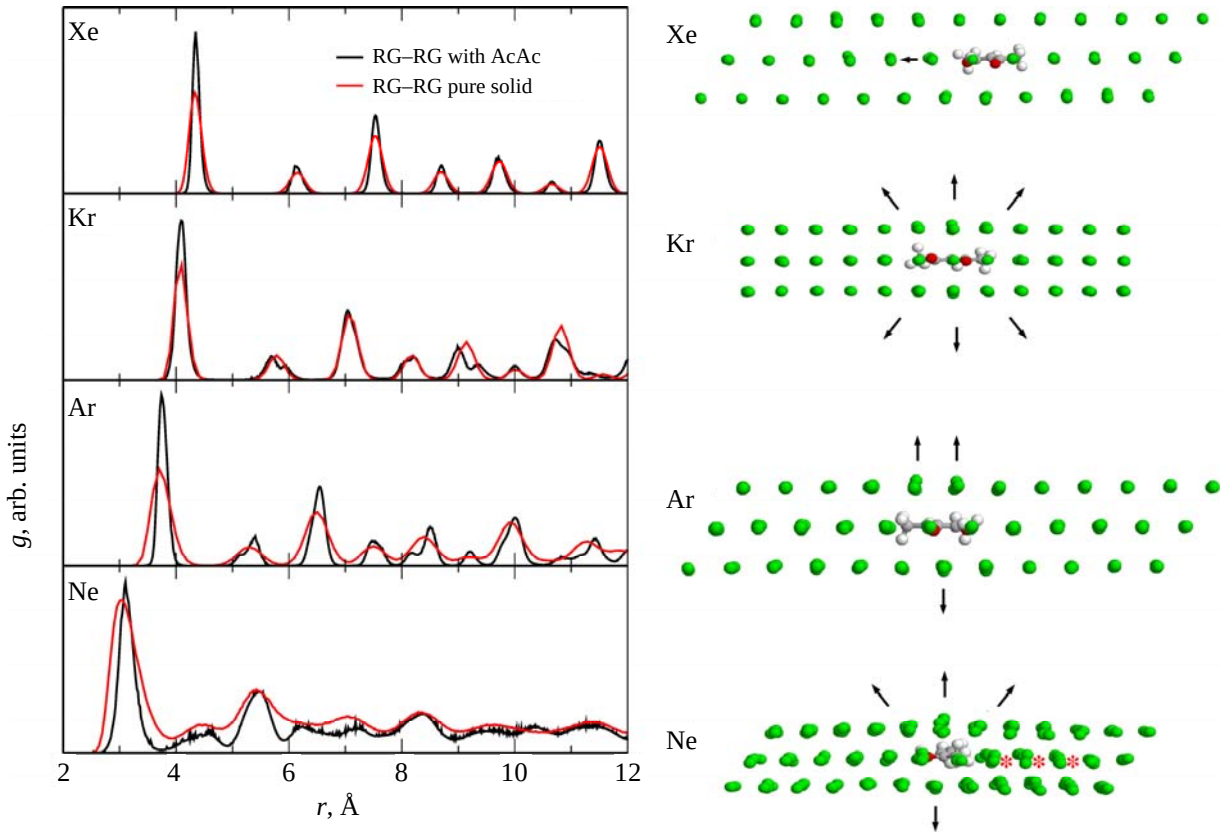

Fig. 5. (Color online) Left panel: RG–RG radial distribution function $g(r)$ in pure rare gas solids (red solid lines) and in AcAc doped matrices (black solid lines). Right panel: local deformation of the lattice around AcAc. The strong deviation experienced by some rare gas atoms close to the impurity is shown with arrows. Some atomic rearrangements are underlined with an (*) symbol showing the extent of the perturbation in Ne matrices. The RG atoms are shown in green, oxygens in red, carbons in grey and hydrogens in white.

The positions of the minima in the O–Kr and C–Kr interaction potentials are also close to the equilibrium position in the Kr–Kr potential, but these interactions are stronger and their contributions explain the shift to lower energies observed in Fig. 6. Interestingly, the O–Xe and C–Xe contributions at the equilibrium position are smaller than in Kr and very close to the contributions in Ar crystals, what could explain a higher solvation energy in Xe than in Kr. This behavior is also observed for 2ClMA and AcAc molecules (top and middle panels of Fig. 6).

The solvation energies for 2ClMA in RG solids (middle panel of Fig. 6) are lower than for MA. In Ne matrices a single band associated to 5v+2 (001) sites appears. A main band with shoulders at each side is observed in Ar solids.

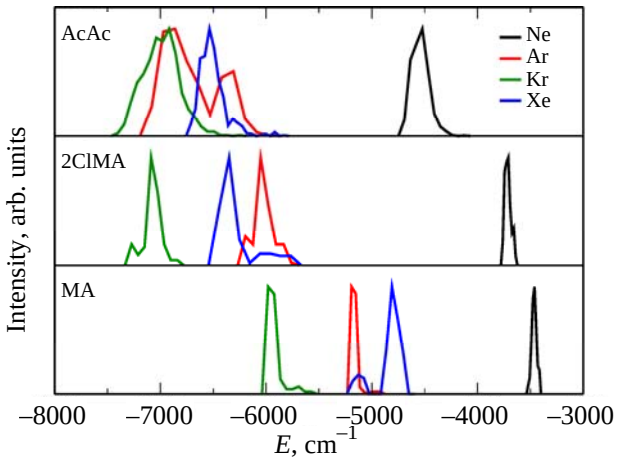

Fig. 6. (Color online) Histograms of "solvation" energies. Intensities are rescaled to fix, for each matrix, the maximum value of the contribution to one, in order to maximize the details in the figure.

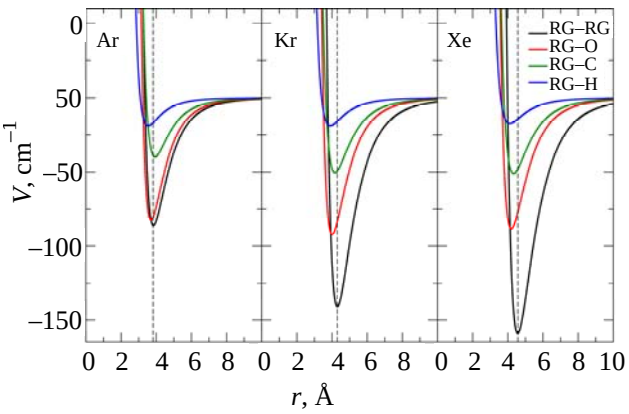

Fig. 7. (Color online) Interatomic pair potentials used for MA/RG samples. Dashed lines are placed at the equilibrium position of RG–RG potentials.

The contributions of the different sites overlap. Two bands are observed in the case of Kr, at lower energy than in Ar: a major band corresponding to 4v (001) sites, and a minor one, at lower energy, to 3v+1 (111) sites. The solvation energies in Xe are close to the energies observed in Ar. Two broad bands appear: a minor one correlated to 3v (001) sites and a major one, at the lowest energy, associated with the 3v (111) sites.

In the case of AcAc/RG, the bands in the histogram show a broadening indicating the contributions of more different environments (top panel of Fig. 6). In Ne matrices a single broad band is observed, at lower energies than in the cases of MA and 2ClMA. The contributions of the different sites overlap, thus no clear correlations are made. Two broad bands are observed in the case of Ar matrices. The band at lower energy corresponds to 4v and 5v (111) sites, while the other correlates to the sites formed in (001) crystallographic planes. In Kr matrices a broad complex band is observed as a result of the site contribution overlap. The site contributions of AcAc in Xe matrices have also a strong overlap, which leads to a difficult correlation of the bands observed in the histogram with the site structure.

Generally, there is a clear correlation between the trends observed for the solvation energies histogram (Fig. 6) and the relative populations of the preferred crystallographic planes (Table 1). One can notice that the solvation energies in sites located in (111) planes are usually lower than in sites located in (001) planes, in agreement with the fact that (111) planes are the most compact planes in the fcc structure. The solvation energy plays an important role in the stabilization of the trapped molecules in each site. In fact, the energy related to the matrix perturbation was not computed because as it has been found in previous reports [9], it has a minor importance regarding the stabilization of the guest molecule.

4.1. Comparison with experiments

The spectroscopy of MA and AcAc has been extensively studied in different cryogenic matrices, including the rare gas family [21,22]. However, no extensive discussion on site effects has been published. Some insight for site effects on these two molecules embedded in Ne, Ar and Xe matrices can be found in Aurelien Trivella PhD Thesis [23].

The author claims that no remarkable differences in the band shape and response to annealing process are observed for the chelated and non-chelated forms of AcAc. This result is consistent with the results obtained through our MD simulations (Table 1 and Fig. 6). A distribution of different occupied sites is observed for this molecule, with similar energetic stabilities. This can explain the absence of annealing effects whereas the molecule is trapped in several families of sites.

In the case of MA a different behavior was observed for Ne in one side and Ar and Xe on the other. Intense and narrow bands were reported for the second group, while large bands were observed in Ne. Similarities in Ar and Xe solids are also obtained in our MD simulations, in terms of solvation energies, whilst MA occupies mainly different crystallographic planes in each case. In Ne solids only one kind of site is populated. The simulations show that MA is located in Ne matrices along the (001) plane removing 4 Ne atoms of that plane, but from 0 up to 2 Ne atoms can also be removed from the nearest adjacent parallel crystallographic planes to accommodate the molecule. This leads to the formation of 4v, 5v and 6v trapping sites with similar energies.

On the other hand, vibrational spectroscopies (FT-IR and Raman) of 2ClMA in rare gas matrices clearly show the presence of sites effects in Ar matrices and not in Ne [10]. IR spectra in Kr and Xe matrices have been recently recorded (not published). Bands in Kr exhibit a structure showing a major and a minor component which can be correlated with the most and the least populated sites obtained in simulations. Spectra in Xe do not highlight any site effect. In the case of Ne matrices 2ClMA removes 5 RG atoms from the (001) crystallographic plane where it is located, and 2 atoms from adjacent planes, forming 7v trapping sites (Table 1). Two major sites were observed in Ar, which could correspond to the two kinds of crystallographic planes occupied by the molecule. In Xe, one crystallographic plane is much more occupied than the other and the first experimental data could only show the spectra in the most populated trapping site. The comparison between MA and 2ClMA in terms of tunneling effect due to the proton transfer in the intramolecular hydrogen bond can be tentatively related to the kind of trapping sites occupied by the molecule: similar sites in Ne with large deformations of the crystallographic ordering around the impurity, to be related to the absence of tunneling splitting in MA/Ne and 2ClMA/Ne samples on one hand, and different sites in Ar with MA mainly trapped in (111) crystallographic planes and 2ClMA trapped both in (001) and (111) planes, to be related to the observation of a tunneling splitting of vibrational levels only in the case of 2ClMA/Ar on the other hand [10].

5. Conclusions

The OM/RG simulated crystals using a deposition model complete the rare gas series for matrix-isolated MA, 2ClMA and AcAc allowing a full comparison among these systems. Simulations show that MA is mainly trapped in 4v+2 (001), 3v (111), 3v (111) and 2v (001) sites in Ne, Ar, Kr and Xe matrices, respectively, and 2ClMA in 5v+2 (001), 4v+2 (001), 4v (001) and 3v (111) sites in the same RG series, highlighting the effect of the chlorine substitution. The larger long-range Cl–RG interactions is responsible of the increment of the RG atoms removed to locate the guest molecule in the matrix. AcAc is preferably located forming 5v+2 (111), 5v+1 (111), 3v (001) and 3v (111) sites. In this case the extension of the molecule is not the only important factor, the role of the methyl hydrogens lying out of AcAc backbone plane has also to be taken into account.

Simulations show good qualitative agreement with IR experiments, indicating the presence of site effects on the spectroscopy of MA in Ne matrices, as well as 2ClMA in Ar crystals. The dispersion in different sites is more important for AcAc.

Acknowledgments

G. Rojas-Lorenzo and A. Gutiérrez Quintanilla want to acknowledge the support of the Programa Nacional de Ciencias Básicas (PNCB: P223LH001-108). G. Rojas-Lorenzo thanks the fruitful help of Anabel Lam Barandela.

1. B. Healy and J.G. McCaffrey, *J. Chem. Phys.* **110**, 3903 (1999).
2. B. Healy, P. Kerins, and J.G. McCaffrey, *Fiz. Nizk. Temp.* **38**, 860 (2012) [*Low Temp. Phys.* **38**, 679 (2012)].
3. V.A. Bracken, P. Gürtler, and J.G. McCaffrey, *J. Chem. Phys.* **107**, 5290 (1997).
4. R. Fraenkel and Y. Haas, *Chem. Phys.* **186**, 185 (1994).
5. R. Fraenkel and Y. Haas, *Chem. Phys. Lett.* **220**, 77 (1994).
6. C. Crépin, P. de Pujo, B. Bouvier, V. Brenner, and Ph. Millié, *Chem. Phys.* **272**, 243 (2001).
7. R. Fraenkel, D. Schweke, Y. Haas, F. Molnar, D. Horinek, and B. Dick, *J. Phys. Chem. A* **104**, 3786 (2000).
8. M. Ryan, M. Collier, P. de Pujo, C. Crépin, and J.G. McCaffrey, *J. Phys. Chem. A* **114**, 3011 (2010).
9. A. Kyrychenko and J. Waluk, *J. Chem. Phys.* **119**, 7318 (2003).
10. A. Gutiérrez-Quintanilla, M. Chevalier, R. Platakyte, J. Ceponkus, G.A. Rojas-Lorenzo, and Claudine Crépin, *Phys. Chem. Chem. Phys.* **20**, 12888 (2018).
11. K.F. Niebel and J.A. Venables, in: *Rare Gas Solids*, M.L. Klein and J.A. Venables (eds.), Academic Press, New York (1976).
12. T. Kihara and S. Koba, *J. Phys. Soc. Jpn.* **7**, 348 (1952).
13. B.W. van der Waal, *Phys. Rev. Lett.* **67**, 3263 (1991).
14. N.W. Ashcroft and N.D. Mermin, *Solid State Physics*, Holt, New York (1976).
15. G. Rojas-Lorenzo, J. Rubayo-Soneira, and S.F. Alberti, *Chem. Phys.* **362**, 34 (2009).
16. R. Lozada-García, G. Rojas-Lorenzo, C. Crépin, M. Ryan, and J. G. McCaffrey, *J. Phys. Chem. A* **119**, 2307 (2015).
17. J.R. Maple, M.-J. Hwang, T.P. Stockfisch, U. Dinur, M. Waldman, C.S. Ewig, and A.T. Hagler, *J. Comput. Chem.* **15**, 162 (1994).
18. H. Sun, S.J. Mumby, J.R. Maple, and A.T. Hagler, *J. Am. Chem. Soc.* **116**, 2978 (1994).
19. L. Uranga-Pina, A. Martinez-Mesa, J. Rubayo-Soneira, and G. Rojas-Lorenzo, *Chem. Phys. Lett.* **429**, 450 (2006).
20. J.P. Bergsma, P.H. Berens, K.R. Wilson, D.R. Fredkin, and E.J. Heller, *J. Phys. Chem.* **88**, 612 (1984).
21. T. Chiavassa, P. Roubin, L. Pizzala, P. Verlaque, A. Allouche, and F. Marinelli, *J. Phys. Chem.* **96**, 10659 (1992).
22. T. Chiavassa, P. Verlaque, L. Pizzala, and P. Roubin, *Spectrochimica Acta A* **50**, 343 (1994).
23. A. Trivella, PhD. Thesis, Université de Marseille (2006).

Теоретичне дослідження «пасток» в кріогенних затверділих інертних газах, допованих молекулами β-дікарбоніла

G. Rojas-Lorenzo, M. Lara-Moreno, A. Gutiérrez-Quintanilla, M. Chevalier, C. Crépin

Для імітації росту допованих кристалів інертного газу використана модель осадження. В якості домішок розглянуто органічні молекули з одним внутрішньомолекулярним водневим зв'язком: малональдегід, 2-хлормалональдегід та ацетилацетон. Залежно від властивостей кристала інертного газу, а також розмірів й форм молекул домішок отримано характеристики різних «пасток». Моделювання проводилося з використанням методів класичної молекулярної динаміки, включаючи ангармонічне наближення, з урахуванням нульових коливань кристала. Результати корелюють з отриманими раніше для цих систем даними ІЧ-спектроскопії.

Ключові слова: кристали інертних газів, атомні та молекулярні домішки, міжатомні парні потенціали, спектроскопія.

Теоретическое исследование «ловушек» в криогенных отвердевших инертных газах, допированных молекулами β-дикарбонила

G. Rojas-Lorenzo, M. Lara-Moreno, A. Gutiérrez-Quintanilla, M. Chevalier, C. Crépin

Для имитации роста допированных кристаллов инертного газа использована модель осаждения. В качестве примесей рассмотрены органические молекулы с одной внутримолекулярной водородной связью: малональдегид, 2-хлормалональдегид и ацетилацетон. В зависимости от свойств кристалла инертного газа, а также размеров и форм молекул примесей получены характеристики различных «ловушек». Моделирование проводилось с использованием методов классической молекулярной динамики, включая ангармоническое приближение, с учетом нулевых колебаний кристалла. Результаты коррелируют с полученными ранее для этих систем данными ИК-спектроскопии.

Ключевые слова: кристаллы инертных газов, атомные и молекулярные примеси, межатомные парные потенциалы, спектроскопия.